Development 124, 113-123 (1997)
Printed in Great Britain © The Company of Biologists Limited 1997
DEV2117

Specific and redundant functions of *Gli2* and *Gli3* zinc finger genes in skeletal patterning and development

Rong Mo[1], Anne Marie Freer[1], Dawn L. Zinyk[1,2], Michael A. Crackower[2,5], Jacques Michaud[3,†], Henry H.-Q. Heng[5], Ki Wai Chik[6], Xiao-Mei Shi[5], Lap-Chee Tsui[2,5], Shuk Han Cheng[6], Alexandra L. Joyner[2-4,††] and Chi-chung Hui[1-3,‡,*]

[1]Program in Developmental Biology and Division of Endocrinology, Research Institute, The Hospital for Sick Children, 555 University Avenue, Toronto, Ontario M5G 1X8, Canada
[2]Department of Molecular and Medical Genetics, University of Toronto, Ontario, Canada
[3]Samuel Lunenfeld Research Institute, Mount Sinai Hospital, Toronto, Ontario M5G 1X5, Canada
[4]Skirball Institute of Biomolecular Medicine, New York University, New York, USA
[5]Department of Genetics, Research Institute, The Hospital for Sick Children, Toronto, Canada
[6]Department of Paediatrics, Chinese University of Hong Kong, Shatin, Hong Kong

*Author for correspondence (e-mail: cchui@sickkids.on.ca)
[†]Present address: Institut D'Embryologie Cellulaire et Moléculaire Du Collège De France et du CNRS, 49 bis, avenue de la Belle Gabrielle, 94736 Nogent-sur-Marne, France
[††]Present address: Skirball Institute of Biomolecular Medicine, New York University, New York, USA
[‡]Present address: Program in Developmental Biology and Division of Endocrinology, Research Institute, The Hospital for Sick Children, 555 University Avenue, Toronto, Ontario M5G 1X8, Canada

SUMMARY

The correct patterning of vertebrate skeletal elements is controlled by inductive interactions. Two vertebrate *hedgehog* proteins, Sonic hedgehog and Indian hedgehog, have been implicated in skeletal development. During somite differentiation and limb development, Sonic hedgehog functions as an inductive signal from the notochord, floor plate and zone of polarizing activity. Later in skeletogenesis, Indian hedgehog functions as a regulator of chondrogenesis during endochondral ossification. The vertebrate *Gli* zinc finger proteins are putative transcription factors that respond to Hedgehog signaling. In *Drosophila*, the *Gli* homolog *cubitus interruptus* is required for the activation of *hedgehog* targets and also functions as a repressor of *hedgehog* expression. We show here that *Gli2* mutant mice exhibit severe skeletal abnormalities including cleft palate, tooth defects, absence of vertebral body and intervertebral discs, and shortened limbs and sternum. Interestingly, *Gli2* and *Gli3* (C.-c. Hui and A. L. Joyner (1993). *Nature Genet.* 3, 241-246) mutant mice exhibit different subsets of skeletal defects indicating that they implement specific functions in the development of the neural crest, somite and lateral plate mesoderm derivatives. Although *Gli2* and *Gli3* are not functionally equivalent, double mutant analysis indicates that, in addition to their specific roles, they also serve redundant functions during skeletal development. The role of *Gli2* and *Gli3* in Hedgehog signaling during skeletal development is discussed.

Key words: skeletal development, Sonic hedgehog, Indian hedgehog, *Gli*, mouse

INTRODUCTION

The vertebrate skeleton is derived from three embryologically distinct lineages through two types of bone development (Erlebacher et al., 1995). The neural crest gives rise to the branchial arch derivatives of the craniofacial skeleton, the sclerotome generates most of the axial skeleton and the lateral plate mesoderm forms the bones of the sternum and limbs. The flat bones of the skull as well as the new bones added to the outer surfaces of the long bones are formed by intramembraneous ossification in which mesenchymal precursor cells differentiate directly into bone-forming osteoblasts. The rest of the skeleton is formed by endochondral ossification where mesenchymal cells condense and differentiate into chondrocytes forming a cartilaginous skeleton which is subsequently transformed into a calcified skeleton. Later in development, longitudinal bone growth also proceeds through endochondral ossification in the growth plates at the epiphyses.

The correct patterning of skeletal elements is controlled by inductive interactions. The apical ectodermal ridge (AER) and zone of polarizing activity (ZPA) signal the growth and pattern formation of the developing limbs (reviewed by Cohn and Tickle, 1996). Signals from the notochord and floor plate direct the formation of sclerotome from the somites (reviewed by Christ and Ordahl, 1995). Epithelial-derived signals are required for the differentiation of facial cartilage (reviewed by Langille and Hall, 1993). Embryological explant studies have recently identified some of these signals – the AER signals are probably fibroblast growth factors (FGFs) and the signals from

the ZPA, notochord and floor plate are likely the secreted factor Sonic hedgehog (SHH) (see Cohn and Tickle, 1996).

Relatively little is known about the nuclear factors that respond to these secreted factors. The paired box containing transcription factor Pax1 has been shown to be induced by SHH during sclerotome differentiation (Fan and Tessier-Lavigne, 1994; Johnson et al., 1994) and is a key nuclear factor in mediating the notochord and floor plate signals (Koseki et al., 1993; Dietrich et al., 1993). Mutations in *Pax1* results in multiple abnormalities of the vertebral column including defects of the vertebral body, absent or reduced intervertebral discs, and absent or reduced ribs (Wallin et al., 1994; Dietrich and Gruss, 1995). In the developing limbs, homeobox genes situated 5′ in the *Hoxa* and *Hoxd* clusters are activated in response to FGF and SHH (Niswander et al., 1994; Laufer et al., 1994). These genes are initially expressed in overlapping domains centered on distal and posterior-distal regions of the limb (Dolle et al., 1989; Haack and Gruss, 1993) and are likely downstream mediators of the AER and ZPA signals. Inactivation of some of these *Hox* genes in mice have revealed their roles in limb development (detailed by Davis and Capecchi, 1996 and Fromental-Ramain et al., 1996). Furthermore, the analysis of compound mutants revealed synergistic limb malformations not present in the single mutants, indicating both specific and redundant functions of these *Hox* genes in limb development. Other homeobox genes, such as *Msx1*, *Msx2* and *MHox*, have also been implicated as regulators of inductive events during skeletal development (see Satokata and Maas, 1994; Martin et al., 1995). Gene disruption in mice has indicated that *Msx1* is required for normal development of the craniofacial skeleton (Satokata and Maas, 1994) and *MHox* plays a regulatory role in the growth of both chondrogenic and osteogenic precursors (Martin et al., 1995).

Members of the *Gli* gene family are potential mediators of SHH signaling during skeletal development. In both humans and mice, three closely related *Gli* genes, *Gli1*, *Gli2* and *Gli3* (Ruppert et al., 1988; Hui et al., 1994), encode zinc finger containing proteins that show significant sequence similarity to the product of the *Drosophila* segment polarity gene *cubitus interruptus* (*ci*; Orenic et al., 1990). Genetic analysis indicates that *ci* functions as a downstream mediator of *hedgehog* (*hh*) signaling (Forbes et al., 1993; Johnson et al., 1995; Motzny and Holmgren, 1995; Dominguez et al., 1996) as well as a repressor of *hh* expression (Dominguez et al., 1996). Extrapolating from these *Drosophila* observations, the *Gli* genes might be expected to play a similar role in signaling by vertebrate *hh* homologs such as SHH.

At the onset of gastrulation, the three mouse *Gli* genes are broadly expressed in the ectoderm and mesoderm (Hui et al., 1994). They are later expressed in the developing somites and limb, where SHH is a key inductive signal. During skeletogenesis, *Gli1* expression is found in the condensing mesenchyme (blastema) and later is restricted to the perichondrium (Walterhouse et al., 1993; Hui et al., 1994). *Gli2* and *Gli3* are coexpressed during mesoderm differentiation – their expression can first be found in the undifferentiated mesenchyme and later in the mesenchyme surrounding the blastema but becomes undetectable upon the completion of organogenesis (Schimmang et al., 1992; Hui and Joyner, 1993; Hui et al., 1994). All three *Gli* genes are also expressed in the neural crest derivatives of the craniofacial skeleton (Hui et al., 1994).

Molecular analyses of the human malformation disorder Greig cephalopolysyndactyly syndrome (GCPS) and the mouse limb mutant *extra-toes* (*Xt*) have revealed a role of *Gli3* in skeletal development (Vortkamp et al., 1991, 1992; Schimmang et al., 1992; Hui and Joyner, 1993). Loss of one copy of the human *GLI3* gene (Vortkamp et al., 1991) results in craniofacial abnormalities such as frontal bossing and a broad nasal root as well as limb defects including preaxial and postaxial polysyndactyly of the hands and preaxial polysyndactyly of the feet in GCPS patients (Gollop and Fontes, 1985). Heterozygous *Xt* mice show craniofacial and limb phenotypes similar to those seen in GCPS patients. We and others have shown that the original *Xt* allele contains a 5′ deletion in *Gli3* (Schimmang et al., 1992; Vortkamp et al., 1992) and the *XtJ* allele contains a 3′ non-overlapping deletion in *Gli3* (Hui and Joyner, 1993). Both *Xt* homozygotes completely lack *Gli3* expression indicating that the dominant phenotypes observed in heterozygous *Xt* mutant mice and GCPS patients are due to haploinsufficiency of *Gli3* (*GLI3*). Hereafter, the *Xt* allele will be designated as $Gli3^{Xt}$ and the *XtJ* allele as $Gli3^{XtJ}$. $Gli3^{Xt}$ homozygotes show a high incidence of neural tube closure defects and severe forebrain malformation (Johnson, 1967; Franz, 1994). They die at birth with severe defects in their craniofacial, axial and appendicular skeletons including an enlarged maxillary region, open skull vault, severe fore limb polydactyly, tibial hemimelia, an unfused sternum, and fusion of neural arches (Johnson, 1967). However, only a subset of *Gli3*-expressing tissues are affected in *Gli3* null mutant animals suggesting that *Gli1* and/or *Gli2* may partially compensate for loss of *Gli3* activity. To study the role of *Gli2* in skeletal development, we have generated a targeted deletion of the zinc finger domain by homologous recombination in embryonic stem (ES) cells. We report here that mutant mice deficient for *Gli2* and *Gli3* exhibit different subsets of skeletal defects. While double homozygous *Gli2*;*Gli3* mutants die before the onset of skeletogenesis, mutations of *Gli2* and *Gli3* show synergistic effects in compound mutants indicating that *Gli2* and *Gli3* have specific as well as redundant functions in skeletal development.

MATERIALS AND METHODS

Generation of the $Gli2^{zfd}$ mutation

The human *GLI2* gene was mapped to chromosome 2q14.1-21 and the mouse *Gli2* gene was localized to chromosome 1E2-4 by fluorescence in situ hybridization (data not shown). The targeting vector was constructed from two overlapping mouse genomic clones that contain the *Gli2* zinc finger domain isolated from a 129/Sv genomic library. To construct the targeting vector, a 2.5 kb *Xba*I 5′ homology fragment was subcloned into the *Xba*I site of pPNT (Tybulewicz et al., 1991). Subsequently, a 5 kb *Bam*HI-*Xba*I fragment of 3′ homology was cloned into the *Xho*I site of the above subclone. Both the PGKneo and PGKtk cassettes are in opposite transcriptional orientation compared to the endogenous *Gli2* gene. The culture, selection and electroporation of R1 ES cells was carried out as described by Wurst and Joyner (1993). ES cell colonies that are resistant to 150 μg/ml of G418 and 2 μM ganciclovir were analyzed by Southern blotting for homologous recombination events. Genomic DNA was prepared directly from 96-well plates for restriction enzyme digestion as described by Hogan et al. (1994). Genomic DNA was digested with *Eco*RV and hybridized with a 0.7 kb *Xba*I-*Bam*HI 5′ probe, or with *Bam*HI and hybridized with a 1.0 kb *Xba*I-*Eco*RI 3′ probe. Chimeras were generated by ES-morula aggregration with targeted ES lines (Nagy et al., 1994). Chimeric males

were bred to CD1 or 129/Sv females to establish F_1 heterozygotes. Genotypes of *Gli2^{zfd}* mutant embryos and animals were determined by Southern blot analysis of tail DNA or by PCR analysis of ear punch or yolk sac (Hogan et al., 1994). The following primers (sense *Gli2* primer: 5′AAACAAAGCTCCTGTACACG3′; antisense *Gli2* primer: 5′CACCCCAAAGCATGTGTTTT3′; pPNT primer: 5′ATGCCTGCTCTTTACTGAAG3′) were used to detect a 0.3 kb wild-type band and a 0.6 kb mutant band. Samples were amplified for 30 cycles (95°C 80 seconds; 58°C 60 seconds; 72°C 90 seconds).

Gli3^{XtJ} mutant mice

Gli3^{XtJ} mice in a C3H background were obtained as heterozygotes from the Jackson laboratory (Bar Harbor, Maine) and maintained in a (C3H×CD1) F_2 background. The genotypes of heterozygous and homozygous *Gli3^{XtJ}* mice were determined by their characteristic limb phenotypes (Johnson, 1967; Hui and Joyner, 1993).

Generation of *Gli2^{zfd}*;*Gli3^{XtJ}* double mutants

Initial intercrosses between single *Gli2^{zfd}* and *Gli3^{XtJ}* heterozygotes were performed to generate double heterozygotes. Double heterozygotes were mated and progenies were analyzed by skeletal staining. Genotypes of the double mutants were determined by using PCR analysis of yolk sac DNA and phenotypic analysis of the limbs as described above for the single mutants.

Histological and skeletal analyses

Animals were mated overnight and females examined for a vaginal plug the following morning. Noon of the day of evidence for a vaginal plug was considered day 0.5 post coitum (p.c.). Specimens (embryos or skinned fetuses) were either fixed in Bouin's solution or phosphate-buffered 4% paraformaldehyde. Following fixation, specimens were rinsed with H_2O to remove excess picric acid, or phosphate-buffered saline to remove paraformaldehyde, dehydrated through increasing concentrations of ethanol, equlibrated in xylene, impregnated with paraffin wax, embedded, and sectioned at 6 μm. Sections were stained with hematoxylin and eosin.

The cartilaginous skeleton of day 14.5 p.c. mutant embryos (*Gli2^{zfd}*/*Gli2^{zfd}* [*n*=13], *Gli3^{XtJ}*/*Gli3^{XtJ}* [4], *Gli2^{zfd}*/+;*Gli3^{XtJ}*/+ [7], *Gli2^{zfd}*/*Gli2^{zfd}*;*Gli3^{XtJ}*/+[3] and *Gli2^{zfd}*/+;*Gli3^{XtJ}*/*Gli3^{XtJ}* [6]) was analyzed by alcian blue staining (Jegalian and De Robertis, 1992). Skeletal analyses of fetuses and newborn animals were performed by using alcian blue/alizarin red bone staining (Lufkin et al., 1992); *Gli2^{zfd}*/*Gli2^{zfd}* (day 17.5 p.c. [12], day 18.5 p.c. [15] and newborn [7]), *Gli3^{XtJ}*/*Gli3^{XtJ}* (day 18.5 p.c. [4] and newborn [10]), *Gli2^{zfd}*/+;*Gli3^{XtJ}*/+ (day 18.5 p.c. [12]), *Gli2^{zfd}*/*Gli2^{zfd}*;*Gli3^{XtJ}*/+ (day 18.5 p.c. [11]) and *Gli2^{zfd}*/+;*Gli3^{XtJ}*/*Gli3^{XtJ}* (day 18.5 p.c. [5]).

In situ hybridization analysis

In situ hybridization analysis was carried out as described (Hui and Joyner, 1993). The in situ probes used were *Shh* (Echelard et al., 1993) and the three *Gli* genes (Hui et al., 1994).

RESULTS

Gli2^{zfd} mutant mice

To study the function of *Gli2*, we generated a targeted mutation in ES cells by homologous recombination. A positive/negative targeting vector (Fig. 1A) containing 2.5 kb of 5′ and 5.0 kb of 3′ genomic sequences was designed such that homologous recombination would delete a 2.4 kb region of *Gli2* that contains the exons coding for zinc fingers 3-5 as well as 71 amino acid residues carboxyl to the zinc fingers, replacing this DNA with the PGKneo cassette from the pPNT vector (Tybulewicz et al., 1991). Such a deletion would result in an out-of-frame mutation to the sequences 3′ to the deletion. A truncated protein would be made that should not be able to bind DNA since zinc fingers 4 and 5 are known to be important for DNA binding (Pavletich and Pabo, 1993; Zarkower and Hodgkin, 1993). This allele is referred to as *Gli2^{zfd}* (zinc finger deletion). The linearized targeting vector was electroporated into ES cells and clones were selected for resistance to G418 and ganciclovir (see Materials and Methods). 340 double resistant clones were analyzed by Southern blot using a 3′ external probe and 16 cell

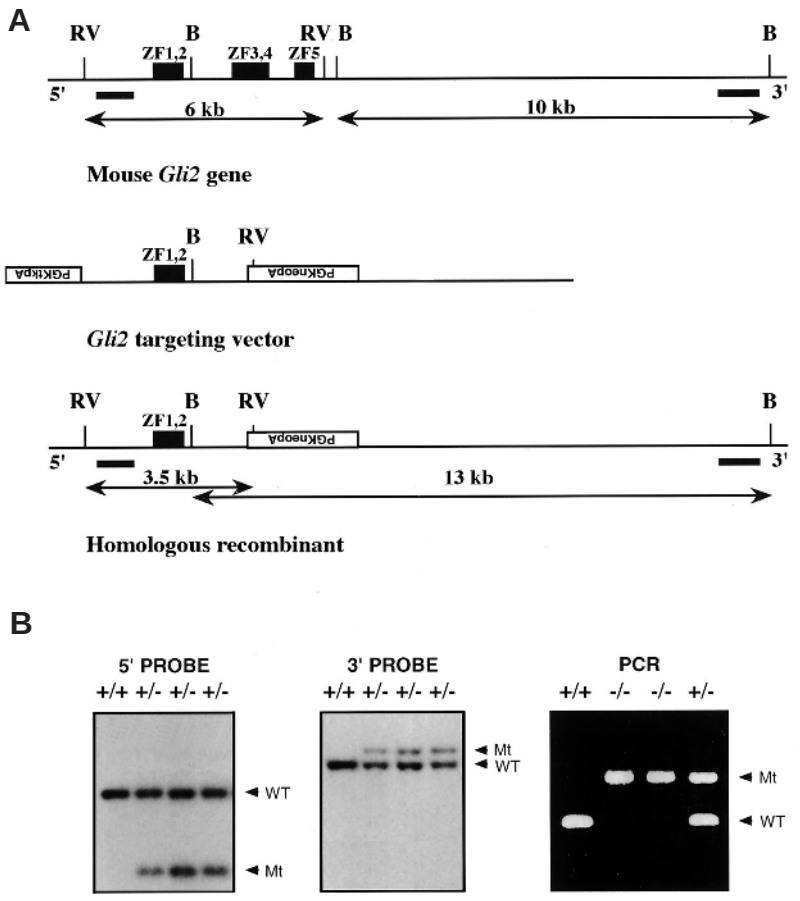

Fig. 1. Targeted disruption of the *Gli2* gene. (A) The targeting vector contains 7.5 kb of genomic sequence of the *Gli2* locus. The black boxes represent the 5 zinc fingers. The 5′ and 3′ probes used for Southern blot analysis are indicated. Homologous recombination replaces zinc fingers 3-5 with the PGKneo gene, resulting in a change in size of the *Eco*RV fragment detected by the 5′ probe from 6 kb (WT) to 3.5 kb (Mt). Similarly, the *Bam*HI fragment detected by the 3′ probe shifts from 10 kb (WT) to 13 kb (Mt). (B) Southern blot and PCR analyses. Southern blot analysis of DNA from control R1 (+/+) and three targeted (+/–) ES lines. The wild-type (WT) and mutant (Mt) DNA fragments detected by the 5′ and 3′ probes are as described in A. Also shown is PCR analysis of yolk sacs from wild type (+/+), heterozygous (+/–) and homozygous (–/–) embryos. The wild-type (WT) band is 0.3 kb and the mutant (Mt) band is 0.6 kb.

lines including G3 and G10 yielded the 13 kb *Bam*HI band expected from a homologous recombination event (Fig. 1B). The 3.5 kb *Eco*RV band expected from a homologous recombination event was detected by a 5′ internal probe (Fig. 1B). The G3 and G10 targeted ES cell lines were used to generate chimeras by ES cell-morula aggregation (Nagy et al., 1994). These chimeras transmitted the mutation to their progeny. G3 was backcrossed to CD1 for two to four generations while G10 was maintained in a 129/Sv background. Similar phenotypes were obtained with mouse lines generated from each of the two clones.

Heterozygous *Gli2*^{zfd} mutant mice do not show any detectable abnormalities. Heterozygous mice were intercrossed to generate homozygous mutant animals. Analysis of more than 500 offspring from heterozygous intercrosses at weaning did not reveal any homozygous mutant animals. When newborn animals were analyzed from these crosses, many stillborn pups were found and most of them were genotyped as homozygous *Gli2*^{zfd} mutants (see Table 1). Analysis of homozygotes at various developmental stages (days 9.5-19.5 p.c.) revealed that they were present in the expected Mendelian ratio of roughly 25%. The percentage of homozygotes became somewhat lower at day 18.5 p.c. and at birth, suggesting that some lethality occurred during later embryonic development. Consistent with this, we frequently observed resorbed embryos at late gestational stages.

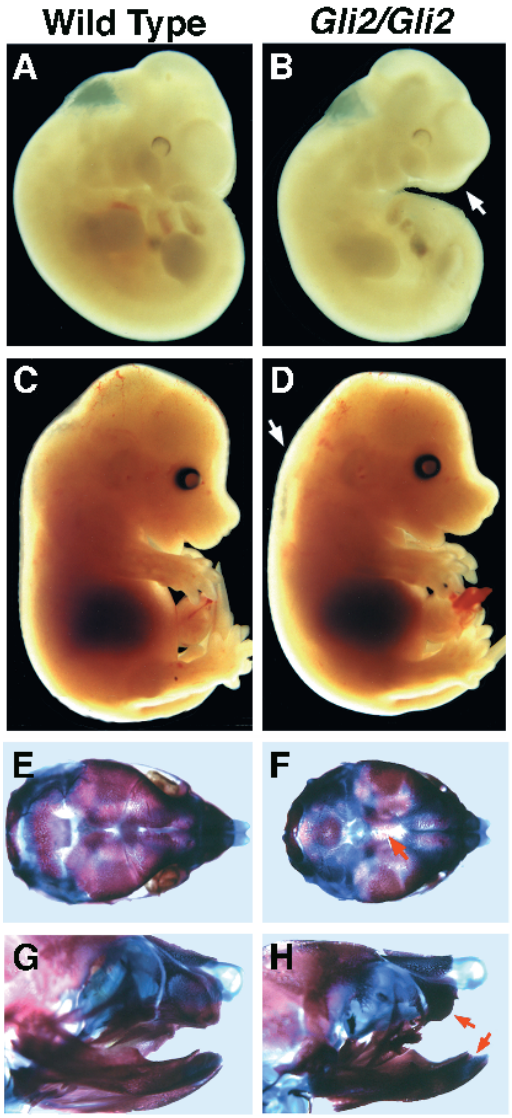

Fig. 2. Craniofacial abnormalities in homozygous *Gli2*^{zfd} mutants. Lateral views of day 10.5 p.c. wild-type (A) and homozygous *Gli2*^{zfd} (B) embryos show that the mutant is smaller than the wild-type littermate and exhibits microcephaly (indicated by the arrow). Later at day 14.5 p.c. (C,D), homozygous *Gli2*^{zfd} mutants (D) show edema at the back (arrow) and the head appears to be flattened. At birth (E-H), skeletal staining reveals that the skull is shortened in homozygous *Gli2*^{zfd} mutants (F) and, in some homozygous *Gli2*^{zfd} mutants (H), both upper and lower incisors are missing (indicated by the arrows).

Craniofacial abnormalities in homozygous *Gli2*^{zfd} mutants

Homozygous *Gli2*^{zfd} mutants could be first recognized at day 10.5 p.c. by their small size and microcephaly (Fig. 2A,B). At day 14.5 p.c., their heads appeared to be flattened and they frequently showed subcutaneous edema in the back (Fig. 2C,D). Craniofacial abnormalities could be clearly seen in homozygous *Gli2*^{zfd} mutants at late gestational periods. In the skull, a deficiency of the medial portion of the frontal and parietal bones is observed in most mutants (Fig. 2E,F). The mutants also showed delayed ossification of the skull (Fig. 3C-F). Truncation of the distal maxilla and mandible was partly due to an absence of upper and/or lower incisors (Fig. 2G,H). The alveolar processes, which surround the molars, appear normal although mutant mandibles are reduced in size (see Fig. 8G). 91% (30/33) of the homozygotes did not have an upper incisor and 33% (11/33) did not have a lower incisor. Tympanic ring bones are absent in some mutants indicating that inner ear development is affected by the *Gli2*^{zfd} mutation (Fig. 3C-F).

Many newborn homozygotes have a severely cleft secondary palate (Fig. 3A,B). Analysis of 45 homozygotes by histological sectioning (n=12) or skeletal staining (n=33) enabled us to quantitate the cleft palate defect as 64% penetrant. The palatal phenotype ranged from a complete absence of the presphenoid bone as well as the maxillary and palatine shelves (Fig. 3C) to normal looking palatal shelves (Fig. 3F). Serial coronal sections along the palate at days 13.5 to 14.5 p.c. showed that there was a delay or failure in the elevation of the mutant palatal shelves. At day 13.5 p.c., wild-type shelves are in the process of fusion with a clearly visible midline seam (Fig. 3G) and, by day 14.5 p.c., are properly fused with continuous mesenchyme (Fig. 3K). In contrast, mutant shelves were either not elevated at all (Fig. 3H,L) or were only partially elevated (Fig. 3I,M). Some of the mutant shelves did elevate but showed a delay in fusion (Fig. 3J,N). The former two mutant classes are presumed to develop into the subset of progeny exhibiting cleft palate.

Table 1. Results of *Gli2*^{zfd} heterozygote matings

Age	Litters	+/+ (%)	+/– (%)	–/– (%)
E9.5	5	10 (23)	24 (53)	11 (24)
E10.5	8	18 (21)	45 (53)	22 (26)
E14.5	13	49 (36)	59 (44)	27 (20)
E17.5	12	31 (29)	50 (48)	24 (23)
E18.5	12	38 (31)	63 (52)	20 (17)
Newborn	15	35 (31)	64 (57)	14 (12)

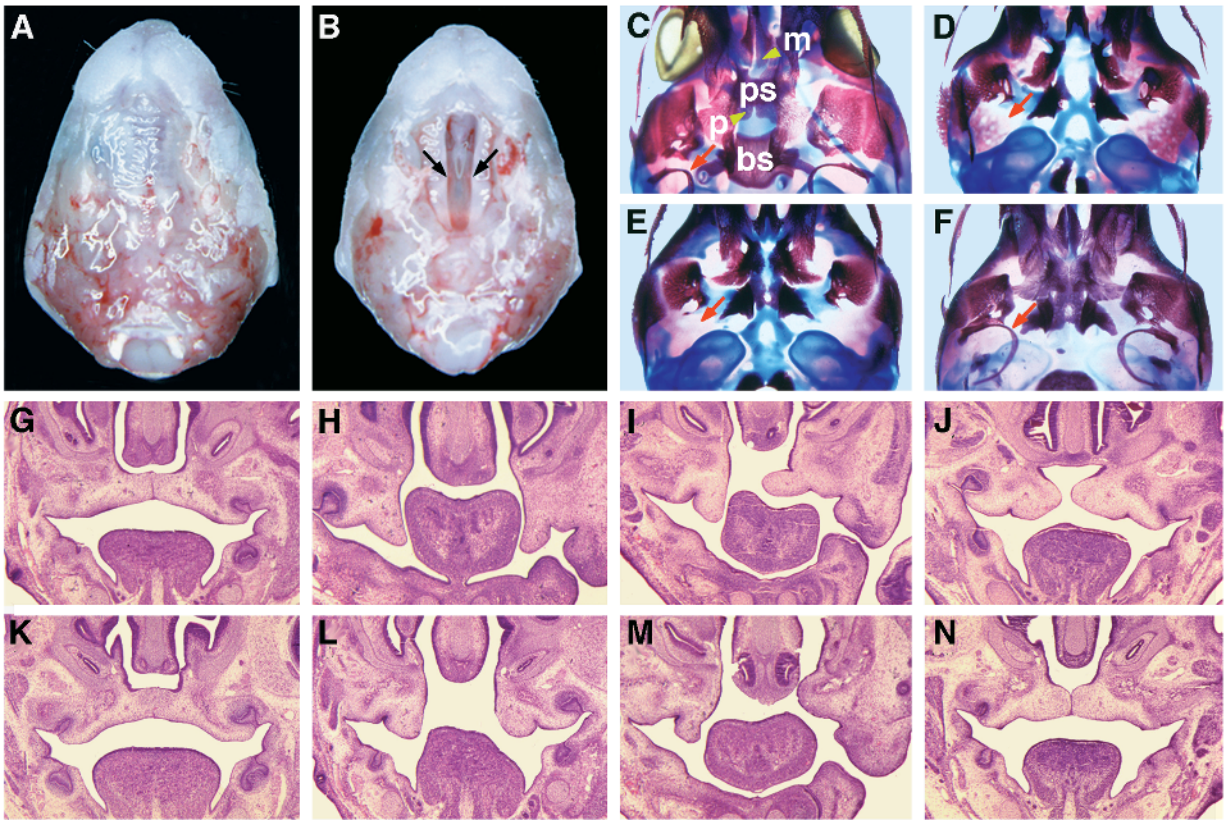

Fig. 3. Cleft palate in homozygous *Gli2*^{zfd} mutant mice is due to abnormal palatal shelf elevation. Ventral view of the upper jaw of wild-type (A) and homozygous *Gli2*^{zfd} (B) neonates. The arrows point to the open nasal cavities. Ventral view of the base of skulls of a wild-type (C) and three homozygous *Gli2*^{zfd} (D-F) neonates. The maxillary (m) and palatine (p) shelves, as well as the presphenoid (ps) and basisphenoid (bs) bones are completely absent in the mutant shown in D but are variably affected in others (E,F). Arrows indicate the tympanic ring which is absent in some *Gli2*^{zfd} mutant mice (D,E). Elevation of palatal shelves is abnormal in homozygous *Gli2*^{zfd} mutant mice. Frontal sections through the heads of days E14.5 (G-J) and E15.5 (K-N) wild-type (G,K) and homozygous *Gli2*^{zfd} (H-J,L-N) embryos illustrate a complete failure (H,L), partial failure (I,M) or delay (J,N) in the elevation of the palatal shelves in the mutants.

Gli3^{XtJ} mutant mice

Johnson (1967) provides a detailed analysis of *Gli3*^{Xt} mutant mice, in which the 5′ region of *Gli3* has been deleted (Schimmang et al., 1992). In this study, we confirm similar skeletal abnormalities in *Gli3*^{XtJ} mutant mice, which contain a 3′ deletion in *Gli3* (Hui and Joyner, 1993). Homozygous *Gli3*^{XtJ} mutants exhibit severe craniofacial abnormalities similar to those reported for *Gli3*^{Xt} homozygotes (Johnson, 1967): an enlarged maxillary region, reduced external nasal processes and failure of skull vault formation. In addition, homozygous *Gli3*^{XtJ} mutants also revealed an incomplete penetrance of cleft palate and tooth defects (data not shown). Consistent with their roles in palatal and tooth development, *Gli2* and *Gli3* are highly expressed in the developing facial mesenchyme (see Fig. 5M,N and unpublished data).

Gli2^{zfd} and *Gli3*^{XtJ} mutant mice exhibit distinct limb and sternal phenotypes

The limbs and sternum are derived from the lateral plate mesoderm. Both structures are severely affected in *Gli3*^{XtJ} mutants (Fig. 4C,F,I). During limb development, undifferentiated mesenchymal cells first aggregrate to form condensations. These prechondrogenic condensations (blastema) then segment and bifurcate along the proximodistal axis to form the stylopods (humerus and femur), the zeugopods (ulna/fibula and radius/tibia), and finally the autopods (carpals, metacarpals and digits). In *Gli3*^{XtJ} mutants, the fore limbs exhibit severe polydactyly (seven to eight digits) and the hind limbs also show polydactyly (six digits). Some *Gli3*^{XtJ} mutants, however, have only five digits in the hind limbs (see Fig. 4F). *Gli3*^{XtJ} mutants also show a severe truncation of the tibia (Fig. 4F) and a slight shortening and thickening of the humerus, ulna and radius (Fig. 4C). These observations indicate that the *Gli3*^{XtJ} mutation severely affects the development of the autopods. While the *Gli3*^{XtJ} mutation has very little effect on the development of stylopods and zeugopods of the fore limbs, it causes deletion of some anterior components in the hind limbs, resulting in tibial hemimelia as well as a mild preaxial polydactyly (Fig. 4F). The sternum of *Gli3*^{XtJ} mutants is unfused (Fig. 4I).

In contrast, except for a delay in the ossification of the digits, *Gli2*^{zfd} mutants show no obvious abnormalities of the autopods (Fig. 4B,E). 100% (12/12) of day 17.5 p.c. mutant skeletons and 53% (8/15) of day 18.5 p.c. mutant skeletons did not show any sign of ossification in their digits. The length of *Gli2*^{zfd} mutant limbs was significantly reduced. When compared with wild type counterparts, the ossification of humerus, ulna and radius was reduced to 75%, 85% and 50%, respectively, and

the ossification of femur, fibula and tibia was reduced to 85%, 75% and 60%, respectively. Although the length of *Gli2^{zfd}* mutant sternums was reduced, ossification of the sternebrae was normal (Fig. 4H). Analysis of cartilaginous skeletons at day 14.5 p.c. confirmed the same phenotypes in both mutants (data not shown).

The different effects of *Gli2^{zfd}* and *Gli3^{XtJ}* mutations on limb development correlate with the differential expression of *Gli2* and *Gli3* during embryogenesis. As shown in Fig. 5, all three *Gli* genes showed a dynamic pattern of expression during limb development. At day 10.5 p.c., while *Gli1* expression is restricted to the distal mesenchyme in the posterior region of the limb buds, *Gli2* and *Gli3* are broadly expressed in the undifferentiated mesenchyme (Fig. 5B-D). Interestingly, a region in the posterior mesenchyme, which corresponds to the zone of polarizing activity and expresses *Shh* (Fig. 5A), consistently shows little or no expression of the three *Gli* genes (indicated by the arrows in Fig. 5A-D). Later in development, *Gli1* expression is found in the condensing mesenchyme and eventually becomes restricted to the perichondrium (Fig. 5F and unpublished data). Although *Gli2* and *Gli3* are both expressed in the mesenchyme surrounding the condensing mesenchyme (Fig. 5G,H,K,L), *Gli3* is expressed at a higher level in the autopods (Fig. 5H,L). Similar expression patterns were observed in both fore limbs and hind limbs (Fig. 5I,J). It is thus possible that the more severe autopod defects observed in *Gli3^{XtJ}* mutants are due to the preferential expression of *Gli3* and functional requirement for *Gli3* in the distal part of the developing limbs.

Vertebral defects in *Gli2^{zfd}* and *Gli3^{XtJ}* mutant mice

The vertebral column is derived from the sclerotome – medially located sclerotome cells contribute to intervertebral discs and vertebral bodies, lateral sclerotome cells form the pedicles and ribs, and the dorsal part of the sclerotome contributes to the neural arches (Verbout, 1985). The development of the four occiptal somites is, however, different; they develop into the basioccipital (the occipital equivalent of a vertebral body) and exoccipital (the occipital equivalent of a neural arch) bones without resegmentation (Theiler, 1988).

In all *Gli2^{zfd}* mutants, the development of the basisphenoid bone (a derivative of the cephalic mesoderm) and the basioccipital bone was affected (Fig. 6B). In the vertebral column, no or little ossification of vertebral bodies could be found (Fig. 6E). Examination of individual mutant vertebrae indicated that the ossification of neural arches was normal (data not shown; see Fig. 6H). Histological sections of *Gli2^{zfd}* mutants revealed that the intervertebral discs were absent or reduced and a bend in the vertebral column frequently occurred in the thoracic-lumbar region (data not shown). In addition, 36% (12/33) of the mutants showed a bilateral pair of extra ribs and 6% (2/33) had an unilateral extra rib (not shown). In contrast to *Gli2^{zfd}* mutants, the basisphenoid bone, basioccipital bone and vertebral bodies developed normally in *Gli3^{XtJ}* mutants (Fig. 6C,F).

In contrast to *Gli2^{zfd}* mutants, all *Gli3^{XtJ}* mutant mice exhibited abnormal development of the neural arches; the C1 and C2 neural arches were fused and the neural arches of other cervical vertebrae were expanded (Fig. 6I). They also showed a bilateral pair of extra ribs (data not shown). Interestingly, though *Gli2* and *Gli3* are both expressed in the developing sclerotome (Hui et al., 1994), *Gli2* is preferentially expressed in the medial sclerotome cells while *Gli3* is preferentially expressed in the dorsal part of the sclerotome (Fig. 5O,P).

Redundant roles of *Gli2* and *Gli3* in skeletal development

To determine whether *Gli2* and *Gli3* play redundant roles in skeletal development, we analyzed the skeletons of double mutant mice at days 14.5 and 18.5 p.c. Double heterozygous mutant mice are viable and were mated to one another. No double homozygotes were found among the six litters killed at day 14.5 p.c. and the eight litters at day 18.5 p.c. (Table 2). Our preliminary results indicated that double homozygotes die before day 10.5 p.c. Skeletal analysis revealed no significant difference between *Gli2^{zfd}*/+;*Gli3^{XtJ}*/+ and *Gli3^{XtJ}*/+ mutants. In contrast, *Gli2^{zfd}*/*Gli2^{zfd}*;*Gli3^{XtJ}*/+ mutants showed an exacerbated phenotype in various skeletal elements. *Gli2^{zfd}*/+;*Gli3^{XtJ}*/*Gli3^{XtJ}* mutants also exhibited some enhancement of the *Gli3^{XtJ}*/*Gli3^{XtJ}* mutant phenotype. These synergistic effects of *Gli2^{zfd}* and *Gli3^{XtJ}* mutations on skeletal development clearly illustrate the redundant functions of *Gli2* and *Gli3*.

Gli3^{XtJ}/+ mutants showed mild preaxial polydactyly in both the fore limbs and hind limbs (Fig. 7F,L). The stylopod and

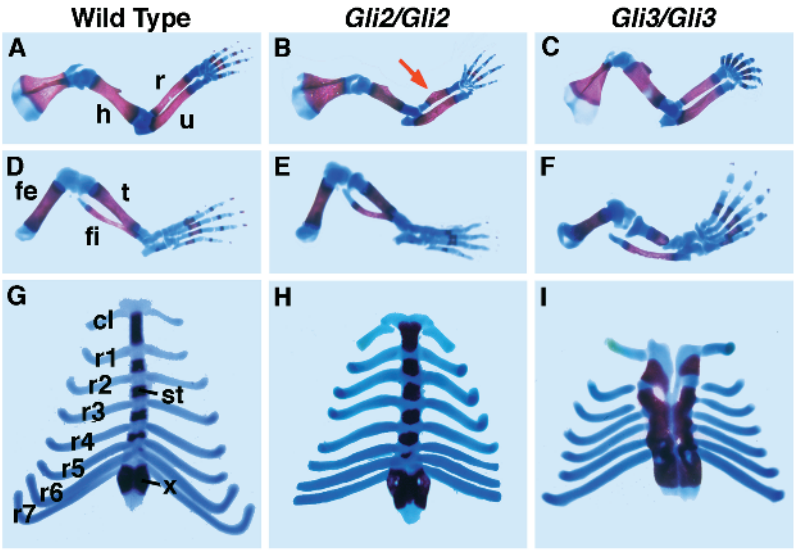

Fig. 4. Limb and sternal defects in homozygous *Gli2^{zfd}* and *Gli3^{XtJ}* mutant mice. The fore limbs (A-C), hind limbs (D-F) and sternum (G-I) of day 18.5 p.c. wild-type (A,D,G), homozygous *Gli2^{zfd}* (B,E,F) and homozygous *Gli3^{XtJ}* (C,F,I) animals are shown. In homozygous *Gli2^{zfd}* animals, the fore limbs show a shortening of humerus (h), radius (r) and ulna (u) and a bowed-shaped radius (indicated by the arrow in B) and the hind limbs show a similar shortening of femur (fe), tibia (t) and fibula (fi) (E). The sternum has seven ribs (r1-r7) attached and the sternabrae (st) and xiphoid (x) are grossly normal (H). In homozygous *Gli3^{XtJ}* animals, the fore limbs show a slight shortening and thickening of humerus, radius and ulna, and severe polydactyly (C) and the hind limbs show a severe truncation of tibia (F). In the hind limbs, the polydactyly is less severe and the anterior part appears to be deleted. The sternum is completely split (I). In this specimen, only the clavicle (cl) and six ribs are attached to the sternum.

Table 2. Results of *Gli2*^{zfd}; *Gli3*^{XtJ} heterozygote matings

Gli2^{zfd}	+/+	+/+	+/+	+/–	+/–	+/–	–/–	–/–	–/–
Gli3^{XtJ}	+/+	+/–	–/–	+/+	+/–	–/–	+/+	+/–	–/–
Expected	6.2	12.5	6.2	12.5	25	12.5	6.2	12.5	6.2
E14.5*	7.3(3)	19.5(8)	9.8(4)	19.5(8)	17.1(7)	14.6(6)	4.9(2)	7.3(3)	0(0)
E18.5†	14.4(13)	21.1(19)	7.8(7)	14.4(13)	15.6(14)	5.6(5)	6.7(6)	14.4(13)	0(0)

Expected percentage assumes Mendelian inheritance of wild-type and mutant alleles. Calculated frequencies of various genotypes are listed with the actual number of animals indicated in brackets.
*6 litters; †8 litters.

zeugopod elements of *Gli3*^{XtJ}/+ mutants were normal (Fig. 7C,I). When compared with *Gli2*^{zfd} homozygotes, *Gli2*^{zfd}/*Gli2*^{zfd};*Gli3*^{XtJ}/+ mutants showed a significant reduction of the stylopod and zeugopod elements in both fore limbs (Fig. 7A,B) and hind limbs (Fig. 7G,H). In particular, the length of radius and tibia appeared to be more reduced than those of ulna and fibula (Fig. 7B,H). These observations suggest that both *Gli2* and *Gli3* are required for the normal development of stylopods and zeugopods. Furthermore, *Gli2*^{zfd}/*Gli2*^{zfd};*Gli3*^{XtJ}/+ mutants exhibited a more severe preaxial polydactyly phenotype (Fig. 7E,F,K,L). In the fore limbs of *Gli2*^{zfd}/*Gli2*^{zfd};*Gli3*^{XtJ}/+ mutants, there was also a postaxial nubbin (Fig. 7E). The lack of a strong autopod phenotype in *Gli2*^{zfd} homozygotes may thus be due to functional redundancy of *Gli2* and *Gli3*.

Functional redundancy of *Gli2* and *Gli3* could also be observed in the development of other skeletal elements, such as the sternum (derived from the lateral plate mesoderm; Fig. 8B), the vertebral column (somite; Fig. 8E) and the mandible (neural crest; Fig. 8H). In contrast to their single mutant counterparts (Fig. 8A,C), *Gli2*^{zfd}/*Gli2*^{zfd};*Gli3*^{XtJ}/+ mutants showed a strong sternum phenotype (Fig. 8B). The sternum was split rostrally and was not properly segmented. As for the limbs, the functional redundancy of *Gli2* and *Gli3* may explain the mild sternum phenotype observed in *Gli2*^{zfd} homozygotes. In the vertebral column, *Gli2*^{zfd} homozygotes showed defects of chondrogenesis ventrally (Fig. 8D) corresponding to the thoracic-lumbar position of the bend of the mutant vertebral column (see above). However, in *Gli2*^{zfd}/*Gli2*^{zfd};*Gli3*^{XtJ}/+ mutants, chondrogenesis was found to be affected in multiple regions along the ventral part of the vertebral column (Fig. 8E). This clearly indicates that *Gli3* also plays a role in the development of the ventral vertebral processes and that the lack of a phenotype in the vertebral bodies of *Gli3*^{XtJ} mutants is due to *Gli2* compensating for the absence of *Gli3*. The mandibles of *Gli2*^{zfd}/*Gli2*^{zfd};*Gli3*^{XtJ}/+ mutants were severely malformed (Fig. 8H). Though *Gli2*^{zfd} homozygotes had a smaller mandible, the development of the coronoid (c),

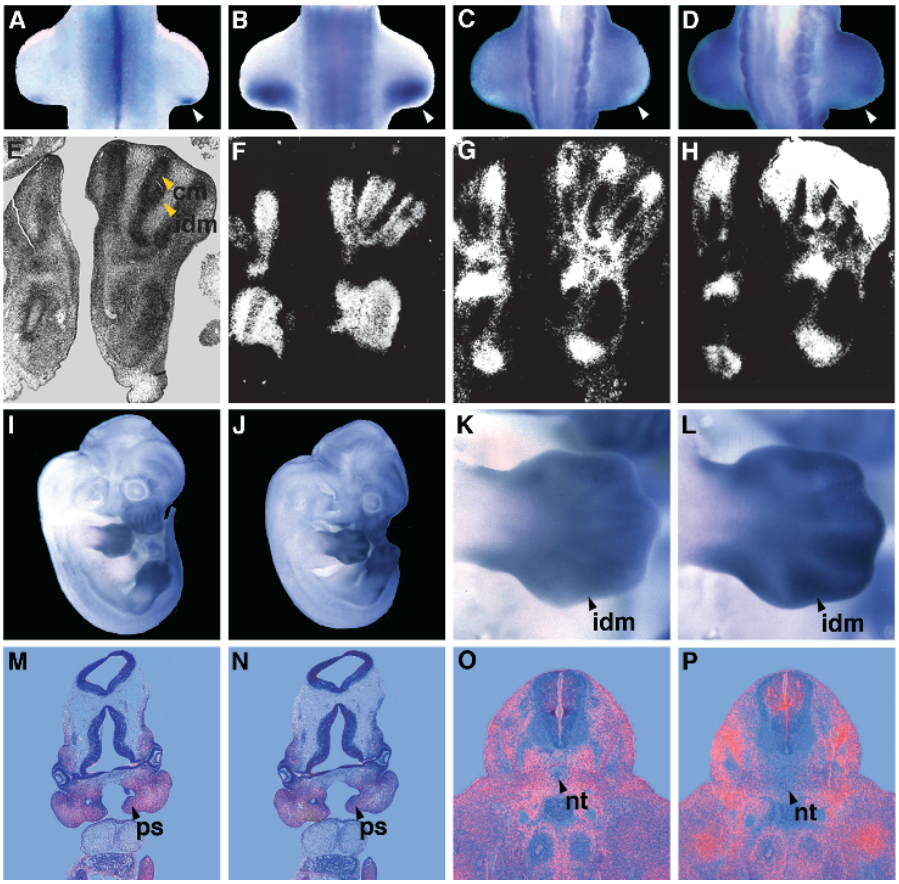

Fig. 5. Differential expression of *Gli2* and *Gli3* during skeletal development. Whole-mount in situ hybridization of day 10.5 p.c. embryos showing the expression of *Shh* (A), *Gli1* (B), *Gli2* (C) and *Gli3* (D) in the fore limb buds. The arrowheads indicate the region, corresponding to the zone of polarizing activity, which shows *Shh* expression and very little or no expression of the three *Gli* genes. (F-H) Adjacent planar sections of the fore limbs from day 12.5 p.c. embryos were hybridized with antisense *Gli1* (F), *Gli2* (G) and *Gli3* (H) probes. The bright-field view is shown in E and dark-field views of the hybridization signals (white) are shown in F-G. *Gli1* expression is restricted to the condensing mesenchyme (cm), whereas *Gli2* and *Gli3* are expressed in the interdigital mesenchyme (idm). Whole-mount in situ hybridization of day 12.5 p.c. embryos reveals the expression of *Gli2* and *Gli3* in the interdigital mesenchyme of both the fore limbs and hind limbs (I-L). Similar to the results shown in G and H, *Gli3* (L) shows a higher level of expression than *Gli2* (K) in the autopods (K,L). (M-P) In situ hybridization on sections of day 11.5 p.c. embryos showing the expression of *Gli2* (M,O) and *Gli3* (N,P) in the developing palatal shelves (ps) (M,N) and vertebral column (O,P). Dark-field views of hybridization signals (red) are overlayed onto bright-field views (blue) of the same section. Note that *Gli2* expression is highly expressed in the medial sclerotomal cells surrounding the notochord (nt) (O), where *Gli3* is expressed at a much lower level (P).

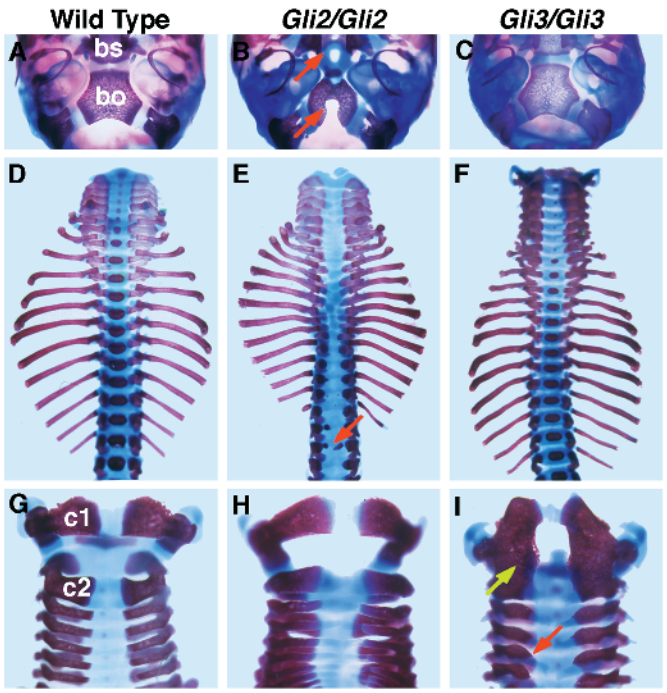

Fig. 6. Vertebral defects in homozygous *Gli2*^{zfd} and *Gli3*^{XtJ} mutant mice. Ventral views of the caudal part of the skull show that the basioccipital (bo) and basisphenoid (bs) bones are severely affected in homozygous *Gli2*^{zfd} animals (indicated by the red arrows; B) but are normal in wild-type (A) and homozygous *Gli3*^{XtJ} (C) animals. Ventral views of the vertebral column show that only very few vertebral bodies (indicated by the red arrow) are present in homozygous *Gli2*^{zfd} animals (E). The intervertebral discs also appear to be malformed in homozygous *Gli2*^{zfd} animals when compared with wild type (D) and homozygous *Gli3*^{XtJ} (F) animals. The neural arches of the cervical vertebrae are well separated and rectangular in shape in both wild-type (G) and homozygous *Gli2*^{zfd} animals (H). In contrast, the neural arches of the first (C1) and second (C2) cervical vertebrae fuse in homozygous *Gli3*^{XtJ} animals (indicated by the yellow arrow; I). Neural arches of other cervical vertebrae also show an irregular shape (red arrow).

condylar (co), angular (a) and dental (d) processes was normal (Fig. 8G). In contrast, all these processes were hypoplastic in *Gli2*^{zfd}/*Gli2*^{zfd};*Gli3*^{XtJ}/+ mutants.

In addition to the fusion of the C1 and C2 neural arches observed in *Gli3*^{XtJ} homozygotes (Fig. 6I), *Gli2*^{zfd}/+;*Gli3*^{XtJ}/*Gli3*^{XtJ} mutants showed neural arch fusion of other cervical vertebrae (not shown). Some *Gli2*^{zfd}/+;*Gli3*^{XtJ}/*Gli3*^{XtJ} mutants also appeared to have more duplicated distal phalanges than others (not shown).

DISCUSSION

Specific and redundant roles of *Gli2* and *Gli3* in skeletal development

We have shown here that *Gli2* is required for normal development of the skeleton. As previously observed in *Gli3* null mutant mice, the disruption of *Gli2* affects some, but not all, of the bones in the craniofacial, axial and appendicular skeletons. In the craniofacial skeleton, *Gli2*^{zfd} mutation affects the development of the basisphenoid bone (a derivative from the cephalic mesoderm), the basioccipital bone (derived from somitic mesoderm), the presphenoid bone, the maxillary and palatine shelves and the incisors (neural crest derivatives). In the axial skeleton, the development of ventral vertebral structures is severely affected with vertebral bodies and intervertebral discs are mostly absent. In the limbs, the stylopod and zeugopod bones are significantly shortened. *Gli2*^{zfd} mutation also results in a shortening of the sternum.

Gli2^{zfd} and *Gli3*^{XtJ} mutants both exhibit an incomplete penetrance of cleft palate and tooth defects. While this can be due to partially redundant functions of *Gli2* and *Gli3* in craniofacial development, it is possible that the genetic background of the mutants (129, C3H and CD1) may contribute to the variation in penetrance and expressivity. Interestingly, other than cleft palate and tooth defects, *Gli2*^{zfd} and *Gli3*^{XtJ} mutations show complete penetrance and affect different subsets of skeletal elements. While the development of the basisphenoid and basioccipital bones appears normal, the skull vault is severely affected in *Gli3* null mutants. In the vertebral column, *Gli3* inactivation affects the development of dorsal structures. The neural arches of all cervical vertebrae tend to fuse with each other. Both the sternum and limb are more malformed in *Gli3* null mutants. Most *Gli3*^{XtJ} homozygotes show a completely split sternum. *Gli3* inactivation causes preaxial polydactyly in both fore limb and hind limb in heterozygous conditions and severe fore limb polydactyly and anterior deletion of the hind limb zeugopod and autopod elements in homozygous conditions. These observations indicate that *Gli2* and *Gli3* play specific roles in skeletal development.

The differential expression of *Gli2* and *Gli3* in the developing limb and sclerotome (Fig. 5) can partly explain why their mutations result in different skeletal malformations. The ventral vertebral defects of *Gli2*^{zfd} homozygotes are reminiscent of those observed in *Pax1* null mutant mice (Wallin et al., 1994; Dietrich et al., 1995). *Pax1* and a closely related gene, *Pax9*, are co-expressed in the developing sclerotome in response to the notochord signals; however, *Pax1* is mainly expressed in medial sclerotomal cells which eventually form the vertebral body and intervertebral discs and *Pax9* in the more lateral regions which give rise to the neural arches (Goulding et al., 1994; Neubuser et al., 1995). Interestingly, *Gli2* is also preferentially expressed in medial sclerotomal cells while *Gli3* is preferentially expressed in the more lateral regions. In correlation with this differential expression, the *Gli2*^{zfd} mutation affects ventral vertebral components and the *Gli3*^{XtJ} mutation affects the dorsal components. Similarly, *Gli3* is strongly expressed in the distal part of the developing limb and *Gli3*^{XtJ} mutation causes severe malformation of the autopods.

The fact that double *Gli2*^{zfd};*Gli3*^{XtJ} homozygotes die around day 10 p.c. before the onset of skeletogenesis strongly suggests that *Gli2* and *Gli3* play redundant roles in embryogenesis. It will be interesting to examine whether *Gli1* also plays redundant roles since all three *Gli* genes are expressed in partially overlapping domains during early embryogenesis (Hui et al., 1994). Our skeletal analyses of double mutant mice have revealed the redundant roles of *Gli2* and *Gli3* in skeletal development. Synergistic malformations were observed in the limb, sternum, vertebral column and mandible of *Gli2*^{zfd}/*Gli2*^{zfd};*Gli3*^{XtJ}/+ mutant mice (Figs 7, 8). Taken together, our

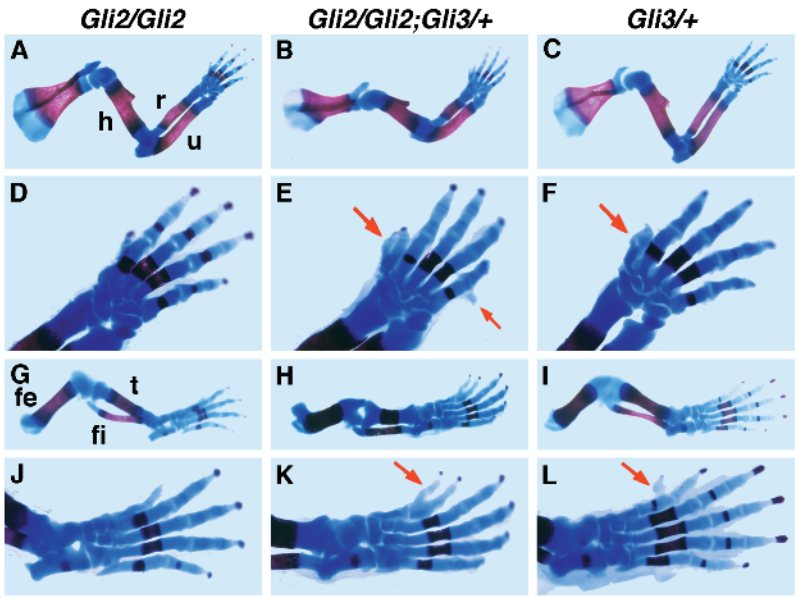

Fig. 7. Exacerbated limb defects in $Gli2^{zfd}/Gli2^{zfd}$;$Gli3^{XtJ}$/+ mutant mice. Both the fore limbs (B,E) and hind limbs (H,K) of $Gli2^{zfd}/Gli2^{zfd}$;$Gli3^{XtJ}$/+ mutant mice show a more severe preaxial polydactyly phenotype than their counterparts in $Gli3^{XtJ}$/+ mutant mice (C,F,I,L). The control is a $Gli2^{zfd}/Gli2^{zfd}$ littermate (A,D,G,J). The preaxial digits are indicated by large arrows (E,F,K,L). The small arrow indicates the postaxial nubbin found in the fore limbs of $Gli2^{zfd}/Gli2^{zfd}$;$Gli3^{XtJ}$/+ mutant mice (E). $Gli2^{zfd}/Gli2^{zfd}$;$Gli3^{XtJ}$/+ mutant mice show a severe truncation of all the long bones (B and H). The anterior zeugopod elements, radius (r) and tibia (t), appear to be most affected. Abbreviations are the same as in Fig. 4.

results indicate that although *Gli2* and *Gli3* exert distinct functions during skeletal development, they also implement partially redundant functions in the development of skeletal elements from all three embryonic lineages (the neural crest, somite and lateral plate mesoderm).

Possible role of *Gli2* and *Gli3* in *hedgehog* signaling

In *Drosophila*, *hh* plays a central role in cell patterning during embryonic and post-embryonic development (Forbes et al., 1993). The *Gli* homolog, *ci*, is an important component of the *hh* pathway. It is required for the activation of *hh* target genes, such as *wingless* (*wg*), *decapentaplegic* (*dpp*) and *patched* (*ptc*) (Motzny and Holmgren, 1995; Johnson et al., 1995; Dominguez et al., 1996). The activity of *ci* is regulated post-transcriptionally. The *hh* signal increases the level of *ci* protein while the *ptc* activity decreases it (Johnson et al., 1995; Dominguez et al., 1996). Increased *ci* protein levels have been shown to induce *dpp* expression in a *hh*-independent manner (Dominguez et al., 1996). Interestingly, besides acting as a downstream mediator of *hh* signaling, *ci* also functions as a repressor of *hh* expression (Domingeuz et al., 1996). In addition to multiple *hh* homologs (Echelard et al., 1993) and the three *Gli* genes described here, several other conserved components of the *hh* pathway have been identified in vertebrates. The vertebrate *ptc* homolog (Goodrich et al., 1996; Margio et al., 1996) and two highly homologous *dpp* homologs, *Bmp2* and *Bmp4* (Bitgood and McMahon, 1995; see Hogan, 1996), are expressed in regions complementary to, or overlapping with, *hh*-expressing cells during embryogenesis. As predicted by the *Drosophila* observations, the expression of the *ptc* homolog, *Bmp2*, and *Bmp4*, can be induced by ectopic *Shh* expression (Goodrich et al., 1996; Margio et al., 1996; Laufer et al., 1994; Niswander et al., 1994; Roberts et al., 1995). Furthermore, the role of cAMP-dependent protein kinase as a negative regulator of the *hh* pathway is conserved in *Drosophila* and vertebrates (Fan et al., 1995; Hynes et al., 1995; Hammerschmidt et al., 1996). These observations strongly suggest that similar signaling mechanisms by *hh*

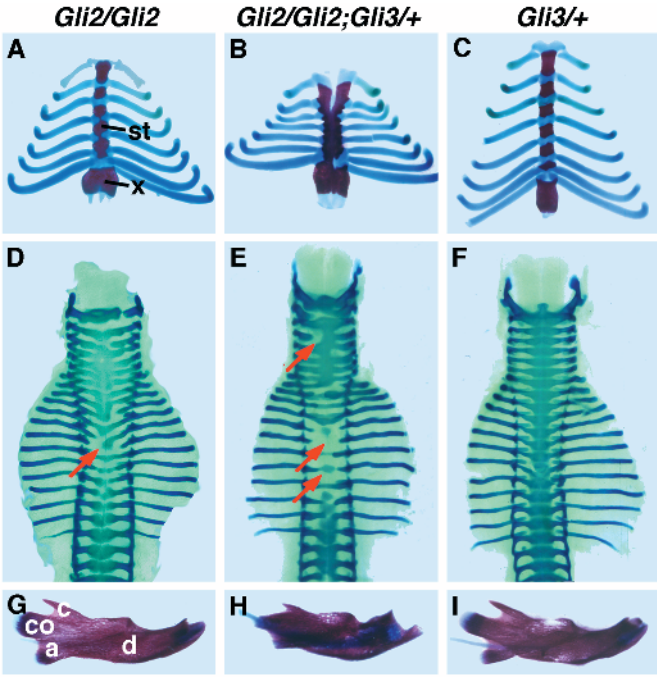

Fig. 8. Defects of the sternum, vertebral column and mandible in $Gli2^{zfd}/Gli2^{zfd}$;$Gli3^{XtJ}$/+ mutant mice. The sternum is severely malformed in $Gli2^{zfd}/Gli2^{zfd}$;$Gli3^{XtJ}$/+ mutant mice (B) when compared with their $Gli2^{zfd}/Gli2^{zfd}$ (A) and $Gli3^{XtJ}$/+ (C) littermates. The sternum is split at the rostral end and the sternabrae are not segmented. In this specimen, only six ribs are attached to the left side of the sternum. (D-F) Alcian blue staining of day 14.5 p.c. embryonic skeletons illustrates severe abnormalities in the chondrogenesis of ventral vertebral components in $Gli2^{zfd}/Gli2^{zfd}$;$Gli3^{XtJ}$/+ mutants (E). $Gli2^{zfd}/Gli2^{zfd}$ mutants (D) show mild defects whereas $Gli3^{XtJ}$/+ mutants (F) appear normal. (G-I) The mandible of $Gli3^{XtJ}$/+ animals (I) is indistinguishable from their wild-type counterparts. Except for a slight reduction of size, the mandibles of $Gli2^{zfd}/Gli2^{zfd}$ mutants (G) appear normal. However, the mandibles of $Gli2^{zfd}/Gli2^{zfd}$;$Gli3^{XtJ}$/+ mutants (H) are severely malformed. The coronoid (c), condylar (co), angular (a) and dental (d) processes are all affected.

homologs may be employed in the induction and morphogenesis of tissues and organs in vertebrates and invertebrates.

Two vertebrate *hh* homologs, *Shh* and *Indian hedgehog* (*Ihh*), have been implicated in skeletal development. During somite development, *Shh* mediates the inductive effects of the notochord in the differentiation of the sclerotome (Fan and Tessier-Lavigne, 1994; Johnson et al., 1994). In the developing limb, *Shh* functions as the ZPA signal in the specification of limb pattern (Riddle et al., 1993; Chang et al., 1994). Expression of *Shh* in the developing tooth and tongue epithelium also suggests that it may function as the inductive signal involved in the epithelial-mesenchymal interactions during tooth and palatal development (Bitgood and McMahon, 1995; Iseki et al., 1996; Koyama et al., 1996; Vaahtokari et al., 1996). During skeletogenesis, *Ihh* is expressed in the pre-hypertrophic regions of the cartilage (Bitgood and McMahon, 1995) and is a regulator of chondrogenesis (Lanske et al., 1996; Vortkamp et al., 1996). If the *hh*/*ci-Hh*/*Gli* signaling pathway is evolutionarily conserved in vertebrates, inactivation of the *Gli* genes should result in (i) defective signaling by *Shh* and *Ihh* as well as (ii) causing ectopic expression of *Shh* and *Ihh*. The results reported here are consistent with both possibilities.

Both single and double mutants of *Gli2* and *Gli3* exhibit clear somite defects. In particular, the disruption of normal *Gli2* function results in a vertebral phenotype similar to that of *Pax1* null mutants. Since *Pax1* is a mediator of *Shh* signaling in the developing sclerotome, our results suggest that *Gli2* can function as a positive regulator of *Pax1*. Since $Gli2^{zfd}/Gli2^{zfd}$;$Gli3^{XtJ}$/+ mutant mice exhibit more severe ventral vertebral defects than $Gli2^{zfd}$ homozygotes, *Gli3* also functions in the reception of the notochord *Shh* signal during sclerotome differentiation, albeit to a lesser extent. Since ectopic expression of *Shh* and *Ihh* in the anterior limb bud induces digit duplication (Riddle et al., 1993; Chang et al., 1994; Vortkamp et al., 1996), the polydactyly phenotype of $Gli3^{XtJ}$ homozygotes may be due to ectopic expression of *hh*. Masuya et al. (1995) reported ectopic expression of *Shh* in $Gli3^{XtJ}$ homozygotes.

Our results thus illustrate both specific and redundant functions of *Gli2* and *Gli3* in skeletal development. Strikingly, the spectrum of skeletal abnormalities is similar to those observed in the nevoid basal cell carcinoma syndrome or Gorlin's syndrome which has recently been shown to be caused by mutation of the human *PTC* gene (Johnson et al., 1996; Hahn et al., 1996). Patients with Gorlin's syndrome have a variety of craniofacial abnormalities, such as cleft palate, cyst jaws and vertebral and limb malformation. Taken together with our observations reported here, these results emphasize the role of the *Hh-Gli/ci-Ptc* pathway in skeletal development. The *Gli2* and *Gli3* mutant mice described here will facilitate the genetic analysis of these pathways in vertebrates.

We would like to thank Malgosia Kownacka, Marina Gertsenstein, Lois Stevenson and Sandra Gardner for their excellent technical assistance, Drs Sean Egan, Howard Lipshitz, Janet Rossant and members of the Hui laboratory for critical reading of the manuscript, and Dr. Andrew McMahon for the *Shh* in situ probe. R.M. is indebted to Dr. York Pei for his financial support. This work was supported by a grant to C.-c. H. from the National Cancer Institute of Canada, with funds from the Terry Fox Run.

REFERENCES

Bitgood, M. J. and McMahon, A. P. (1995). *Hedgehog* and *Bmp* genes are coexpressed at many diverse sites of cell-cell interaction in the mouse embryo. *Dev. Biol.* **172**, 126-138.

Chang, D. T. et al. (1994). Products, genetic linkage and limb patterning activity of a murine *hedgehog* gene. *Development* **120**, 3339-3353.

Christ, B. and Ordahl, C. (1995). Early stages of chick somite development. *Anat. Embryol.* **191**, 381-396.

Cohn, M. J. and Tickle, C. (1996). Limbs: a model for pattern formation within the vertebrate body plan. *Trends Genet.* **12**, 253-257.

Davis, A. P. and Capecchi, M. R. (1996). A mutational analysis of the 5′ *HoxD* genes: dissection of genetic interactions during limb development in the mouse. *Development* **122**, 1175-1185.

Dietrich, S., Schubert, F. R. and Gruss, P. (1993). Altered *Pax* gene expression in murine notochord mutants: The notochord is required to initiate and maintain ventral identity in the somite. *Mech. Dev.* **44**, 189-207.

Dietrich, S. and Gruss, P. (1995). *undulated* phenotypes suggest a role of *Pax-1* for the development of vertebral and extravertebral structures. *Dev. Biol.* **167**, 529-548.

Dollé, P., Izpisua-Belmonte, J.-C., Falkenstein, H., Renucci, A. and Duboule, D. (1989). Coordinate expression of the murine Hox-5 complex homeobox-containing genes during limb pattern formation. *Nature* **342**, 767-772.

Dominguez, M., Brunner, M., Hafen, E. and Basler, K. (1996). Sending and receiving the *hedgehog* signal: control by the *Drosophila* Gli protein cubitus interruptus. *Science* **272**, 1621-1625.

Echelard, Y., Epstein, D. J., St.-Jauques, B., Shen, L., Mohler, J. A., McMahon, J. A. and McMahon, A. P. (1993). Sonic hedgehog, a member of a family of putative signaling molecules, is implicated in the regulation of CNS polarity. *Cell* **75**, 1417-1430.

Erlebacher, A., Filvaroff, E., Gitelman, S. and Derynck, R. (1995). Toward a molecular understanding of skeletal development. *Cell* **80**, 371-378.

Fan, C.-M. and Tessier-Lavigne, M. (1994). Patterning of mammalian somites by surface ectoderm and notochord: evidence for sclerotome induction by a hedgehog homolog. *Cell* **79**, 1175-1186.

Fan, C.-M., Porter, J. A., Chiang, C., Chang, D. T., Beachy, P. and Tessier-Lavigne, M. (1995). Long-range sclerotome induction by Sonic Hedgehog: direct role of the amino-terminal cleavage product and modulation by the cyclic AMP signaling pathway. *Cell* **81**, 457-465.

Forbes, A., Nakano, Y., Taylor, A. and Ingham, P. (1993). Genetic analysis of hedgehog signaling in the *Drosophila* embryo. *Development* **Supplement** 115-124.

Franz, T. (1994). Extra-toes (Xt) homozygous mutant mice demonstrate a role for the Gli-3 gene in the development of the forebrain. *Acta Anat.* **150,** 38-44.

Fromental-Ramain, C., Warot, X., Lakkaraju, S., Favier, B., Haack, H., Birling, C., Dierich, A., Dolle, P. and Chambon, P. (1996). Specific and redundant functions of the paralogous *Hoxa-9* and *Hoxd-9* genes in forelimb and axial skeleton patterning. *Development* **122**, 461-472.

Gollop, T. R. and Fontes, L.R. (1985). The Greig cephalopolysyndactyly syndrome: Report of a family and review of the literature. *Am. J. Med. Genet.* **22**, 59-68.

Goodrich, L. V., Johnson, R. L., Milenkovic, L., McMahon, J. A. and Scott, M. P. (1996). Conservation of the *hedgehog*/*patched* signaling pathway from flies to mice: induction of a mouse *patched* gene by Hedgehog. *Genes Dev.* **10**, 301-312.

Goulding, M., Lumsden, A. and Paquette, A. J. (1994). Regulation of *Pax-3* expression in the dermomyotome and its role in muscle development. **Development 120**, 957-971.

Haack, H. and Gruss, P. (1993). The establishment of murine Hox-1 expression domains during patterning of the limb. *Dev. Biol.* **157**, 410-422.

Hahn, H. et al. (1996). Mutations of the human homolog of Drosophila *patched* in the nevoid basal cell carcinoma syndrome. *Cell* **85**, 841-851 (1996).

Hammerschmidt, M., Bitgood, M. J. and McMahon, A. P. (1996). Protein kinase A is a common negative regulator of Hedgehog signaling in the vertebrate embryo. *Genes Dev.* **10**, 647-658.

Hogan, B., Beddington, R., Constantini, F. and Lacy, E. (1994). Manipulating the mouse embryo. Cold Spring Harbour Laboratory, Second Edition.

Hogan, B. L. M. (1996). Bone morphogenetic proteins: multifunctional regulators of vertebrate development. *Genes Dev.* **10**, 1580-1594.

Hui, C.-c. and Joyner, A. L. (1993). A mouse model of Greig

cephalopolysyndactyly syndrome: the *extra-toes*^{J} mutation contains an intragenic deletion of the *Gli3* gene. *Nature Genet.***3**, 241-246.

Hui, C.-c., Slusarski, D., Platt, K., Holmgren, R. and Joyner, A. L. (1994). Expression of three mouse homologs of the *Drosophila* segment polarity gene *cubitus interruptus*, *Gli*, *Gli-2*, and *Gli-3*, in ectoderm- and mesoderm-derived tissues suggests multiple roles during postimplantation development. *Dev. Biol.* **162**, 402-413.

Hynes, M., Porter, J. A., Chiang, C., Chang, D., Tessier-Lavigne, Beachy, P. A. and Rosenthal, A. (1995). Induction of midbrain dopaminergic neurons by Sonic Hedgehog. *Neuron* **15**, 35-44.

Iseki, S., Araga, A., Ohuchi, H., Nohno, T., Yoshioka, H, Hayashi, F. and Noji, S. (1996). *Sonic hedgehog* is expressed in epithelial cells during development of whsiker, hair, and tooth. *Biochem. Biophys. Res. Comm.* **218**, 688-693.

Jegalian, B. G. and De Robertis, E. M. (1992). Homeotic transformations in the mouse induced by overexpression of a human Hox3.3 transgene. *Cell* **71**, 901-910.

Johnson, D. R. (1967). Extra-toes: a new mutant gene causing multiple abnormalities in the mouse. *J. Embryol. Exp. Morph.* **17**, 543-581.

Johnson, R. L., Laufer, E., Riddle, R. D. and Tabin, C. (1994). Ectopic expression of Sonic hedgehog alters dorsal-ventral patterning of somites. *Cell* **79**, 1165-1173.

Johnson, R. L., Grenier, J. and Scott, M. P. (1995). Patched overexpression alters wing disc size and pattern: transcriptional and post-transcriptional effects on hedgehog targets. *Development* **121**, 4161-4170.

Johnson, R. L. et al. (1996). Human homolog of *patched*, a candidate gene for the basal cell nevus syndrome. *Science* **272**, 1668-1671.

Koseki, H., Wallin, J., Wilting, J., Mizutani, Y., Ebensperger, C., Christ, B. and Balling, R. (1993). *Pax1* as a mediator of notochordal signals in the dorsoventral specification of vertebrae. *Development* **119,** 649-660.

Koyama, E. et al. (1996). Polarizing activity, *Sonic hedgehog*, and tooth development in embryonic and postnatal mouse. *Dev Dyn* **206**, 59-72.

Langille, R. M. and Hall, B. K. (1993). Pattern formation and the neural crest. In *The Skull*, Vol. 1 (ed. J. Hanken and B. K. Hall), pp. 77-111. University of Chicago Press, Chicago.

Lanske, B. et al. (1996). PTH/PTHrP receptor in early development and Indian Hedgehog-regulated bone growth. *Science* **273**, 663-666.

Laufer, E., Nelson, C. E., Johnson, R. L., Morgan, B. A. and Tabin, C. (1994). *Sonic hedgehog* and *FGF-4* act througha signaling cascade and feedback loop to integrate growth and patterning on the developing limb. *Cell* **79**, 993-1003.

Lufkin, T., Mark, M., Hart, C. P., Dolle, P., LeMeur, M. and Chambon, P. (1992). Homeotic transformation of the occipital bones of the skull by ectopic expression of a homeobox gene. *Nature* **359**, 835-841.

Margio, V., Scott, M. P., Johnson, R. L., Goodrich, L. V. and Tabin, C. J. (1996). Conservation in hedgehog signaling: induction of a chicken patched homolog by Sonic hedgehog in the developing limb. *Development* **122**, 1225-1233.

Martin, J. F., Bradley, A. and Olson, E. N. (1995). The *paired*-like homeo box gene *MHox* is required for early events of skeletogenesis in multiple lineages. *Genes Dev.* **9**, 1237-1249.

Masuya, H., Sagai, T., Wakana, S., Moriwaki, K. and Shiroishi, T. (1995). A duplicated zone of polarizing activity in polydactylous mouse mutants. *Genes Dev.* **9**, 1645-1653.

Motzny, C.K. and Holmgren, R. (1995). The Drosophila cubitus interruptus protein and its role in the wingless and hedgehog signal transduction pathways. *Mech. Dev.* **52**, 137-150.

Nagy, A., Rossant, J., Nagy, R., Abramow-Newerly, W. and Roder, J. (1994). Derivation of completely cell culture-derived mice form early-passage. *Proc. Natl. Acad. Sci. USA* **90**, 8424-8428.

Neubuser, A., Koseki, H. and Balling, R. (1995). Characterization and developmental expression of *Pax9*, a paired-box-containing gene related to *Pax1*. *Dev. Biol.* **170**, 701-716.

Niswander, L., Jeffrey, S., Martin, G. R. and Tickle, C. (1994). A positive feedback loop coordinates growth and patterning in the vertebrate limb. *Nature* **371**, 609-612.

Orenic, T. V., Slusarski, D. C., Kroll, K. L. and Holmgren, R. A. (1990). Cloning and characterization of the segment polarity gene cubitus interruptus Dominant of Drosophila. *Genes Dev.* **4**, 1053-1067.

Pavletich, N. P. and Pabo, C. O. (1993). Crystal structure of a five-finger GLI-DNA complex: new perspectives on zinc fingers. *Science* **261**, 1701-1707.

Riddle, R. D., Johnson, R. L., Laufer, E. and Tabin, C. (1993). *Sonic hedgehog* mediates the polarizing activity of ZPA. *Cell* **75**, 1401-1416.

Roberts, D. J., Johnson, R. L., Burke, A. C., Nelson, C. E., Morgan, B. A. and Tabin, C. (1995). Sonic hedgehog is an endodermal signal inducing *Bmp-4* and *Hox* genes during induction and regionalization of the chick hindgut. *Development* **121**, 3163-3174.

Ruppert, J. M., Kinzler, K. W., Wong, A. J., Bigner, S. H., Kao, F.-T., Law, M. L., Seuanez, H.N., O'Brien, S.J. and Vogelstein, B. (1988)**.** The Gli-Kruppel family of human genes. *Mol. Cell. Biol.* **8**, 3104-3133.

Satokata, I. and Maas, R. (1994). *Msx1* deficient mice exhibit cleft palate and abnormalities of craniofacial and tooth development. *Nature Genet.* **6**, 348-355.

Schimmang, T., Lemaistre, M., Vortkamp, A. and Ruther, U. (1992). Expression of the zinc finger gene *Gli3* is affected in the morphogenetic mouse mutant *extra-toes* (*Xt*). *Development* **116**, 799-804.

Theiler, K. (1988). Vertebral malformations. *Adv. Anat. Embryol. Cell Biol.* **112**, 1-99.

Tybulewicz, V. L. J., Crawford, C. E., KJackson, P. K., Bronson, R. T. and Mulligan, R. C. (1991). Neonatal lethality and lymphopenia in mice with a homozygous disruption of the c-abl proto-oncogene. *Cell* **65**, 1153-1163.

Vaahtokari, A., Aberg, T., Jernvall, J., Keranen, S. and Thesleff, I. (1996). The enamel knot as a signaling center in the developing mouse tooth. *Mech. Dev.* **54**, 39-43.

Verbout, A. J. (1985). The development of the vertebral column. *Adv. Anat. Embryol. Cell Biol.* **90**, 1-122.

Vortkamp, A., Gessler, M. and Grzeschik, K.-H. (1991). *GLI3* zinc-finger gene interrupted by translocations in Greig syndrome families. *Nature* **352**, 539-540.

Vortkamp, A., Franz, T., Gessler, M. and Grzeschik, K.-H. (1992). Deletion of *GLI3* supports the homology of the human Greig cephalopolysyndactyly syndrome (GCPS) and the mouse mutant extra toes (Xt). *Mammalian Genome* **3**, 461-463.

Vortkamp, A., Lee, K., Lanske, B., Serge, G. V., Kronenberg, H. M. and Tabin, C. J. (1996). Regulation of rate of cartilage differentiation by Indian Hedgehog and PTH-related protein. *Science* **273**, 613-622.

Wallin, J., Wilting, J., Koseki, H., Fritsch, R., Christ, B. and Balling, R. (1994). The role of *Pax1* in axial skeleton development. *Development* **120**, 1109-1121.

Walterhouse, D., Ahmed, M., Slusarski, D., Kalamaras, J., Boucher, D., Holmgren, R. and Iannaccone, P. (1993). *gli*, a putative zinc finger transcription factor, is expressed in a segmental pattern during normal mouse development. *Dev. Dyn.* **196**, 91-102.

Wurst, W. and Joyner, A. L. (1993). Production of targeted embryonic stem cell lines. In *Gene Targeting: A Practical Approach*, (ed. A.L. Joyner), pp. 31-62. Oxford University Press, Oxford.

Zarkower, D. and Hodgkin, J. (1993). Zinc fingers in sex determination: only one of the two C. elegans Tra-1 proteins binds DNA in vivo. *Nucl.Acids Res.* **21**, 3691-3698.

(Accepted 5 October 1996)